Multimodal Analysis of PEI-Mediated Endocytosis of Nanoparticles in Neural Cells

Cameron W. Evans,[†,‡] Melinda Fitzgerald,[‡] Tristan D. Clemons,[†,‡] Michael J. House,[§] Benjamin S. Padman,[⊥] Jeremy A. Shaw,[⊥] Martin Saunders,[⊥] Alan R. Harvey,[∥] Bogdan Zdyrko,[#] Igor Luzinov,[#] Gabriel A. Silva,[△,▽] Sarah A. Dunlop,[‡] and K. Swaminathan Iyer[†,*]

[†]School of Biomedical, Biomolecular and Chemical Sciences, The University of Western Australia, 35 Stirling Highway, Crawley WA 6009, Australia, [‡]Experimental and Regenerative Neurosciences, School of Animal Biology, The University of Western Australia, Australia, [§]School of Physics, The University of Western Australia, Australia, [⊥]Centre for Microscopy, Characterisation and Analysis, The University of Western Australia, Australia, [∥]School of Anatomy and Human Biology, The University of Western Australia, Australia, [#]School of Materials Science and Engineering, Clemson University, Clemson, South Carolina 29634, United States, [△]Department of Bioengineering, University of California, San Diego, 9500 Gilman Drive, La Jolla, California 92093, United States, and [▽]Department of Ophthalmology, University of California, San Diego, Jacobs Retina Center, 9415 Campus Point Drive, La Jolla, California 92037, United States

ABSTRACT

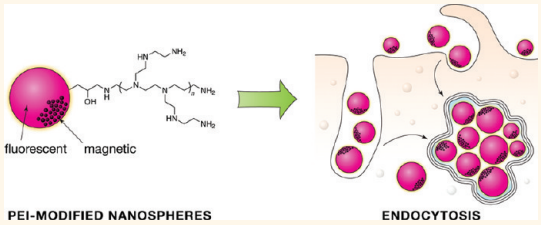

Polymer nanoparticles are widely used as a highly generalizable tool to entrap a range of different drugs for controlled or site-specific release. However, despite numerous studies examining the kinetics of controlled release, the biological behavior of such nanoparticles remains poorly understood, particularly with respect to endocytosis and intracellular trafficking. We synthesized polyethylenimine-decorated polymer nanospheres (*ca.* 100−250 nm) of the type commonly used for drug release and used correlated electron microscopy, fluorescence spectroscopy and microscopy, and relaxometry to track endocytosis in neural cells. These capabilities provide insight into how polyethylenimine mediates the entry of nanoparticles into neural cells and show that polymer nanosphere uptake involves three distinct steps, namely, plasma membrane attachment, fluid-phase as well as clathrin- and caveolin-independent endocytosis, and progressive accumulation in membrane-bound intracellular vesicles. These findings provide detailed insight into how the intracellular delivery of nanoparticles is mediated by polyethylenimine, which is presently the most commonly used nonviral gene transfer agent. This fundamental knowledge may also assist in the preparation of next-generation nonviral vectors.

KEYWORDS: nanosphere · endocytosis · neuron · polyethylenimine · multimodal imaging

The use of nanoparticles for site-specific delivery of therapeutic payloads is a goal that has attracted considerable attention in biomedical research.[1,2] The potential ability to load a single nanoparticle preparation with a variety of drugs and facilitate delivery to specific intracellular or extracellular sites would be a significant advance, because the nanoparticle delivery strategy is generalizable and can be used to release low molecular mass compounds, proteins, and recombinant DNAs at focal areas of disease, maximizing clinical benefits while limiting side effects.[2,3] Recent reports also suggest that nanoparticles can influence cellular signaling by interacting with membrane microdomains that house different signaling components such as receptors, signal activators, and transducers.[2,4−6] Because the response to this activation includes changes to cellular transport and targeting, a precise understanding of the entire intracellular nanoparticle itinerary, beyond the point of initial entry, is important to fully realize the potential of these nanomaterials as drug carriers and transfection agents.

Intracellular and extracellular barriers preventing successful drug delivery have been overcome in numerous studies using nanosized complexes of cationic lipids (lipoplexes) or synthetic polycations (polyplexes).[7−9] Of the latter, polyethylenimine (PEI), the most widely used nonviral vector, is considered the gold standard. This is because PEI can act as a "proton sponge" and promote endosomal escape, resulting in very high transfection efficacy of its polyplexes.[10,11] After endocytosis, the natural acidification within the endosome protonates PEI, inducing chloride ion influx, osmotic swelling, and destabilization of the vesicle, leading to release of polyplexes into the cytoplasm.[12,13] The major shortfall of PEI as a nonviral vector, however, is that

* Address correspondence to swaminatha.iyer@uwa.edu.au.

Received for review June 16, 2011 and accepted October 17, 2011.

Published online October 17, 2011
10.1021/nn2022149

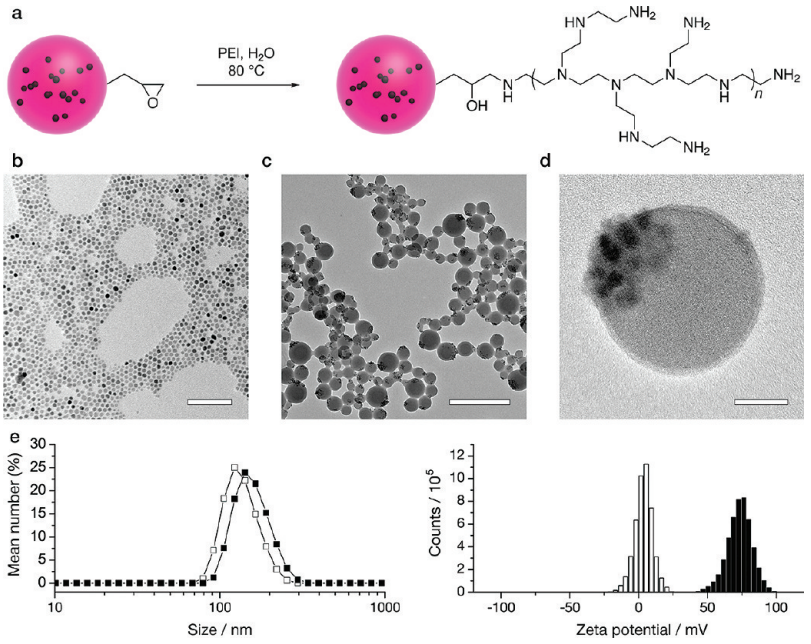

Figure 1. Fluorescent, superparamagnetic nanospheres were prepared by an emulsion route and made use of the reactive epoxide groups of PGMA to anchor PEI. (a) Schematic representation of the attachment of PEI to fluorescent PGMA–RhB nanospheres containing iron oxide nanoparticles. (b) Iron oxide (magnetite, Fe_3O_4) nanoparticles prepared by high-temperature decomposition (scale bar = 100 nm). (c) Low-magnification image of polymeric nanospheres (scale bar = 500 nm). (d) Individual polymer nanosphere showing distribution of iron oxide nanoparticles within the polymer shell (scale bar = 20 nm). (e) Particle size (left panel) and zeta potential (right panel) distributions before (open) and after (solid) modification with PEI.

toxicity scales with transfection efficacy.[11,14] There is very little mechanistic understanding of PEI-mediated intracellular delivery,[15] which is important not only because PEI is commonly used for nonviral gene transfer but also because this knowledge may direct the design and synthesis of next-generation nonviral vectors with low toxicity. Most current methods to study intracellular trafficking of nanoparticles are restricted to co-localization of nanomaterials with specific endocytic markers or the exclusion of specific mechanisms by chemical inhibition or cell mutation.[16–21]

RESULTS AND DISCUSSION

In this work, an approach was developed to directly image endocytosis and intracellular trafficking using fluorescent and magnetic polymer nanospheres. Polymer nanospheres were prepared from poly(glycidyl methacrylate) (PGMA) modified with rhodamine B (RhB) dye, which was used to encapsulate magnetite (Fe_3O_4) nanoparticles. The epoxide groups on PGMA enabled anchoring of PEI chains by means of a simple ring-opening reaction (Figure 1a), as previously demonstrated.[22] These nanospheres enabled a multimodal approach to directly assess how PEI mediates the cellular trafficking of nanoparticles, using correlated relaxometry, fluorescence spectroscopy and microscopy, and transmission electron microscopy. The polymer nanoparticles were synthesized using a nonspontaneous emulsification method, in which a binary solvent mixture containing both immiscible and soluble components was employed as the dispersed phase. This organic solution of the dye-modified polymer, also containing iron oxide nanoparticles (Figure 1b), was emulsified in water in the presence of a surfactant. The polymer nanoparticles were characterized using transmission electron microscopy (Figure 1c, d), dynamic light scattering (Figure 1e), fluorescence spectrophotometry (Figure S1), and magnetometry (Figure S2). Analysis of nanospheres before and after PEI attachment revealed a small increase in average size and a large positive shift in the zeta potential distribution (Figure 1e). The average particle diameter following PEI attachment was 160 nm (distribution 90–260 nm), and particles comprised approximately 3% PEI by weight (see Supporting Information for elemental analysis). Nanospheres were magnetically separated from excess, unbound PEI.

Toxicity of Nanospheres. The toxicity and transfection efficacy of PEI depend on both its molecular weight and structure (*i.e.*, linear or branched).[15] Two possible explanations for cellular perturbation and toxicity have been suggested. First, the presence of free PEI may play a role in inducing cell dysfunction because both branched and linear configurations can bind to plasma membrane proteoglycans, compromise membrane integrity, and induce early necrotic-like changes within 30 min.[14] Second, PEI-induced cytotoxicity has been related to the activation of a mitochondrially mediated apoptotic program involving channel formation in the outer mitochondrial membrane within 24 h.[14,23] In the present study, covalent grafting of PEI chains to the

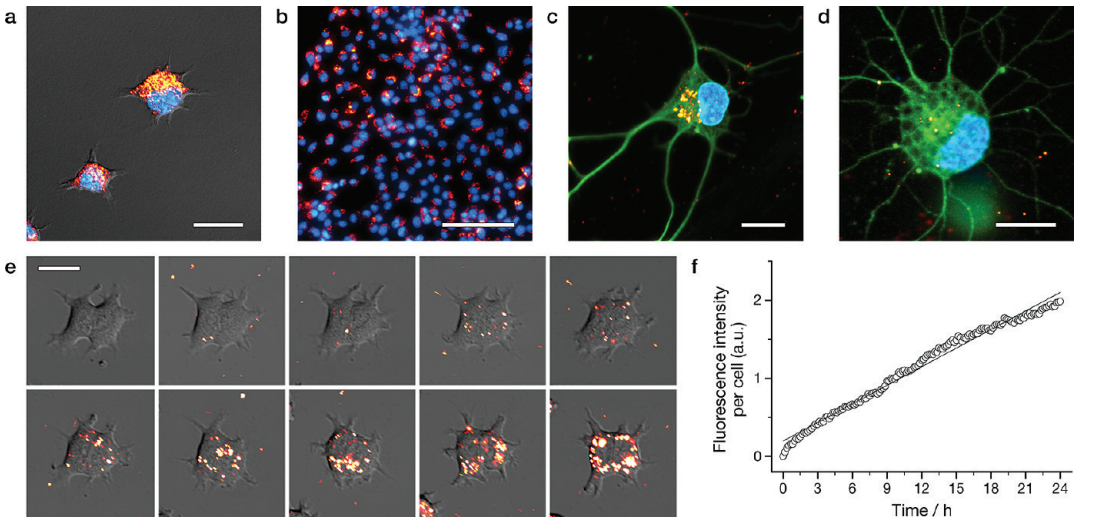

Figure 2. PEI-modified polymeric nanospheres (10 μg mL^{-1}) are rapidly internalized. (a) Confocal maximum intensity projection of nanospheres in PC12 cells after 72 h (red = RhB, nanospheres; blue = Hoechst, nuclei; DIC overlay; 40×/1.25, scale bar = 20 μm). (b) Epifluorescence image of nanosphere uptake in rMC-1 cells after 24 h (red = RhB, nanospheres; blue = Hoechst, nuclei; 20×/0.50, scale bar = 100 μm). (c) Hippocampal neuron as viewed by confocal microscopy after 24 h incubation with nanospheres (red = RhB, nanospheres; green = β-III-tubulin/Alexa 488, neurons; blue = Hoechst, nuclei; 60×/1.49, scale bar = 5 μm). (d) Confocal image of a cortical neuron after 24 h incubation with nanospheres (red = RhB, nanospheres; green = β-III-tubulin/Alexa 488, neurons; blue = Hoechst, nuclei; 60×/1.49, scale bar = 5 μm). (e) Frames from a region of confocal time-lapse experiment (0, 0.5, 1, 2, 3, 6, 9, 12, 18, 24 h) showing internalization of nanospheres by PC12 cells (red = RhB, nanospheres; DIC overlay; 20×/0.75, scale bar = 10 μm). (f) Nanosphere uptake in PC12 cells over time quantified by RhB fluorescence.

magnetic PGMA core allowed the removal of free PEI using magnetic separation, facilitating a clear determination of whether PEI-modified nanospheres were toxic or not.

The toxicity of the modified nanospheres was examined in rat pheochromocytoma neural progenitor (PC12) and retinal Müller glial cell lines (rMC-1), as well as primary rat hippocampal and cortical neuron cultures after 24 and/or 72 h incubation (Figure S3). For the immortalized cultures, there was no decrease in viable cell numbers ($p > 0.05$) for any of the tested concentrations (up to 250 μg mL^{-1}). Similar results were observed in the primary neuron cultures, where a toxic effect ($p \leq 0.05$) was observed only at very high nanosphere concentrations (1000 μg mL^{-1}) that would be inappropriate therapeutically. The assay was verified by assessing trypan blue dye exclusion in PC12 cells. In line with previously proposed mechanisms of PEI toxicity, we suggest two reasons for our observed lack of toxicity in the tested cell lines and primary cultures. First, our PEI chain length was shorter (1.2 kDa) than used in previous studies (25 and 750 kDa),[14,24] and second, PEI was bound to the nanospheres and, as a result, may have been unable to interact with mitochondrial membranes. This investigation covered the time course of known cytotoxic changes.[14]

Nanosphere Uptake Monitored by Fluorescence. Nanosphere uptake was examined in more depth, to further analyze intracellular trafficking and investigate why PEI-modified nanospheres were not toxic. When nanospheres were incubated with PC12 cells, nanospheres with PEI modification were taken up rapidly, within minutes, while those without PEI modification were not associated with cells even after 3 days (Figure S4). Nanospheres that were internalized presented a punctate distribution and were excluded from the nucleus (Figure 2a–d). To examine the dynamics of endocytosis, we used live cell confocal imaging to monitor fluorescence of nanospheres in PC12 cells for periods of 24 and 72 h (Figure 2e, Videos S1 and S2). In time-lapse experiments, using a single confocal slice through the cells, we observed a linear increase in fluorescence per cell with time (Figure 2f). Similar results were obtained with primary cortical and hippocampal neuronal cultures, with a greater intensity of fluorescence per cell in cortical cells (Figure S5). There was no apparent correlation between the intensity of fluorescence indicating nanosphere uptake and the viability of the various cell cultures following treatment. The result in PC12 cells was also confirmed using a spectrofluorometric plate reader to measure intensity over large samples of cells. A constant rate of uptake has been previously reported for zwitterionic quantum dots in HeLa cells.[25]

Endocytosis of Nanospheres Determined by Drug Inhibition and Electron Microscopy. There are many distinct endocytic pathways that coexist in mammalian cells that regulate the entry of a wide range of different sized moieties from ions to macromolecules, pathogens, and drugs. It follows that polymeric nanoparticle drug delivery systems are also subject to the same selectivity.[2,6,26] Uptake of nanoparticles by endocytosis

can occur *via* a number of different routes depending on the cell type and the nature of the cargo (nanoparticle size and surface charge). Pinocytosis, or fluid-phase uptake, has often been reported as a common route for uptake of positively charged macromolecules, comprising macropinocytosis (for particles >1 μm), clathrin-mediated endocytosis ($\leq$120 nm), and caveolin-mediated endocytosis ($\leq$90 nm).[5,7,27−29] In the case of PEI/DNA polyplexes, endocytosis is initiated when polyplexes bind to syndecans, which are negatively charged heparan sulfate proteoglycans (HSPGs) in cell membranes.[30−32] Syndecan clustering around the particle triggers cytoplasmic binding of these transmembrane proteins to actin filaments through linker proteins, which subsequently supports polyplex uptake through endocytic vesicles. More recently, a distinct fluid-phase pathway, independent of clathrin and caveolin, has been identified to contribute to the uptake of PEI-25/DNA polyplexes of size $\geq$150 nm, and importantly, macropinosomes have been reported to have a higher propensity to deliver PEI-25/DNA cargo than endosomes.[27] Consequently, multiple pathways of intracellular trafficking, including macropinocytosis, should be considered in the analysis of PEI-mediated endocytosis of our nanospheres.

The internalization of nanospheres was investigated in PC12 cells following treatment with well-known inhibitors of clathrin-mediated endocytosis (chlorpromazine), lipid raft- and caveolin-mediated endocytosis (nystatin/progesterone), and macropinocytosis (*N*,*N*-dimethylamiloride).[33−37] We observed no statistically significant reductions in uptake ($p > 0.05$) for any of these drugs either individually or in combination (Figure S6). As the uptake of PEI-modified nanospheres was not significantly inhibited by treatment with selected drugs, macropinocytic and clathrin- and caveolin-mediated endocytic routes are probably not required for uptake of polymer nanospheres. Furthermore, the result implies that there is at least one other possible mode of entry for these nanoparticles. It is important to note that the use of inhibitors to identify uptake pathways is not conclusive, however, because such treatment may up-regulate a pathway that is usually silent.[6,19] Up-regulation of nascent pathways has cell-wide consequences in terms of signaling, lipid and protein distributions, membrane tension, and stress responses.[6] Therefore, electron microscopy was used as an additional means of assessing endocytosis as well as the intracellular itinerary of the internalized PEI-modified nanospheres.

Transmission electron microscopy was used to image cellular processes involved in endocytosis and cellular trafficking after 3, 6, 12, 24, and 72 h exposure to nanospheres (Figure 3). In these images, the polymer nanospheres appear as light circles, while the encapsulated iron oxide nanoparticles are much smaller and electron dense, as in Figure 1d. PEI-mediated endocytosis involved adsorption of nanospheres to the cell surface, perhaps suggesting that endocytosis is triggered by interaction with syndecans on the cell membrane as for cationic polyplexes.[30] The number of nanospheres associated with the cell surface increased with time. Nanosphere uptake was accompanied by protrusions and invaginations of the plasma membrane (Figure 3a), characteristic of macropinocytosis, and also tubular invaginations characteristic of clathrin- and caveolin-independent endocytosis[26] extending 0.5−2 μm into PC12 cells (Figure 3b). These observations accord with the results of the chemical inhibition experiment, as nanosphere uptake was not suppressed when macropinocytosis and clathrin- and caveolin-dependent endocytosis were inhibited.

Individual nanospheres were observed throughout the cytoplasm of PC12 cells within 3 h (Figure 3c). After 6 h, nanospheres appeared to have a greater proximity to one another, forming loose clusters that were occasionally membrane-bound. After 12 h, loose clusters were frequently observed near vesicles enclosed by multiple membranes, and by 24 h, these clusters appeared to be mostly membrane-bound. The membrane-bound nanosphere clusters themselves were often grouped together, and in some instances membranes were apparently in the process of fusion (Figure 3d). By 72 h, the clusters were larger (200−500 nm) and comprised several smaller membrane-bound packages that were grouped together and enclosed by one or more membranes (Figure 3d, e). These observations suggested that nanospheres were being captured within endosomes, and the presence of multivesicular bodies indicated endosome maturation.[38,39]

Immunohistochemistry Shows That Nanospheres Are Not in Lysosomes. Lysosomes constitute the final degradative stage in the endocytic journey, vary in size and appearance, and are usually associated with membrane whorls similar to those we observed ultrastructurally.[38] Using the same time points as the TEM experiment, PC12 cells were incubated with nanospheres and analyzed immunohistochemically for lysosomal-associated membrane protein 1 (LAMP-1), a marker of both late endosomes and lysosomes. We did not observe colocalization of nanospheres with LAMP-1 immunopositive intracellular compartments (Figure S7).

It appears that our lack of observed toxicity of the nanospheres is consistent with observations of nanosphere compartmentalization (and increase in the size of these aggregates), rather than osmotic swelling. In the case of polyplexes, buffering of endosomal compartments by polyamines results in increased entry of H^+, with concomitant Cl^- uptake, which in turn promotes osmotic swelling and endosomal leakage or lysis.[13] This destructive process is the mechanism whereby the DNA polyplex escapes lysosomal capture and so accesses the nucleus with gene delivery and

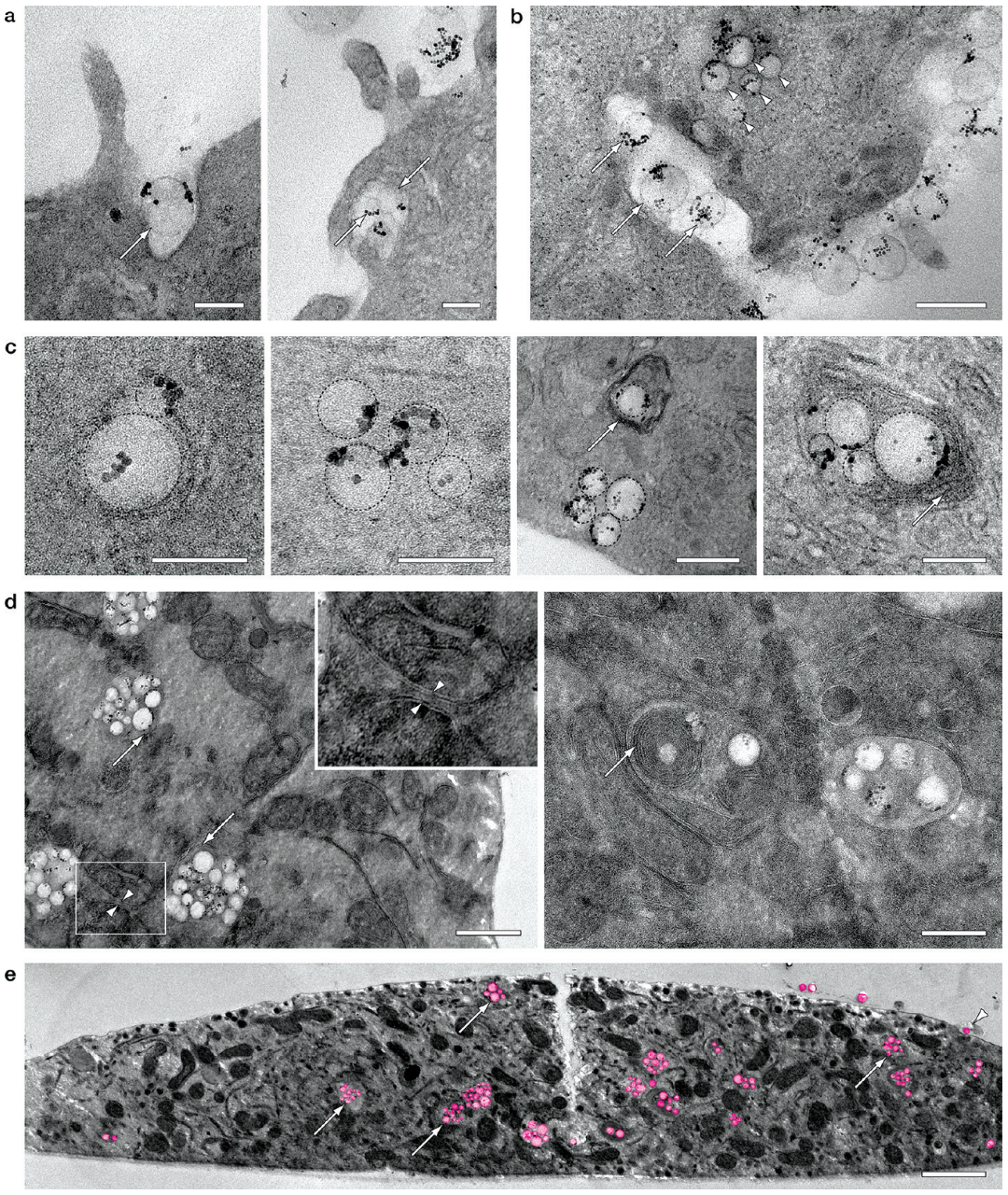

Figure 3. PEI-modified polymer nanospheres (10 μg mL^{-1} in all preparations) are visualized by TEM at various time points displaying stages in internalization and compartmentalization. (a) Endocytosis of nanospheres by a macropinocytotic-like route (nanospheres indicated by arrows; scale bars = 100 nm). (b) Endocytosis that is apparently clathrin- and caveolin-independent (nanospheres indicated by arrows, and internalized particles by arrowheads; scale bar = 200 nm). (c) Time series showing stages in intracellular trafficking. From left to right, at 3 h, nanospheres have been internalized; at 6 h, they form loose clusters; at 12 h, become associated with other membrane-bound vesicles; and at 24 h, are located in clusters bound by multiple membranes (nanospheres are outlined as a visual aid; arrows indicate multiple membranes surrounding nanospheres; scale bars = 100, 100, 200, 100 nm). (d) After 72 h, nanospheres are arranged in discrete clusters, many of which are surrounded by multiple membranes (arrows indicate multiple membranes surrounding nanosphere clusters; arrowheads indicate membranes apparently in the process of fusion, expanded in the inset; scale bars = 200 nm). (e) Whole cell section constructed from three images after 72 h incubation with nanospheres. Nanospheres are visible at the cell surface (arrowhead) and in clusters (arrows) throughout the section (false-colored image; scale bar = 1 μm).

resultant expression. The process is rapid, with release *via* osmotic swelling occurring within 4 h and DNA expression peaking at 24 h.[40] That we did not observe osmotic swelling or signs of endosomal escape is in accordance with our finding of a lack of toxicity within 24 h. Taken together, our observations suggest a sequence in which smaller nanosphere clusters fused to form larger aggregates, but were not contained in lysosomes within 72 h.

Relaxometry Can Be Used to Follow Nanosphere Endocytosis. The observation of compartmentalization of nanospheres in individual PC12 cells by TEM was confirmed

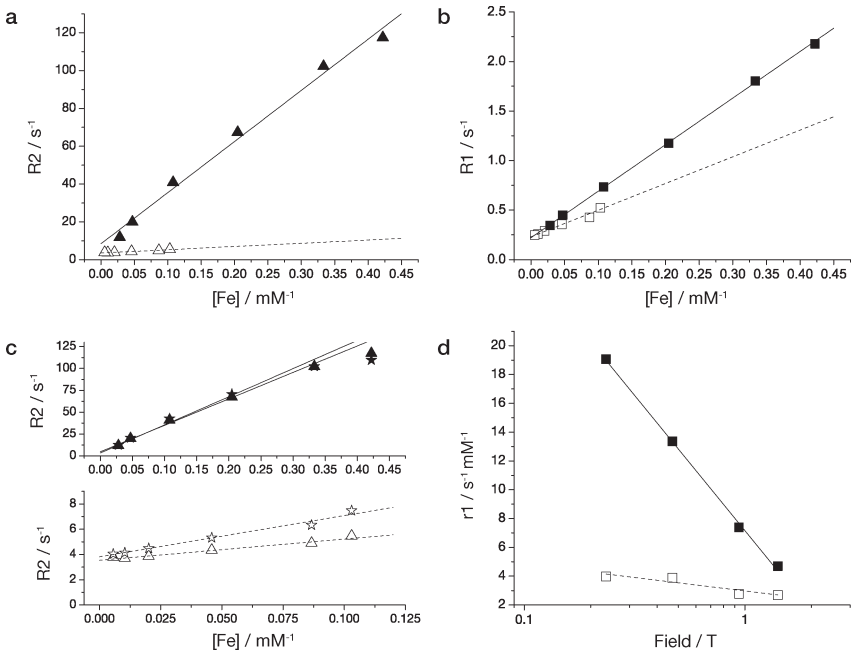

Figure 4. Relaxometry shows effects of compartmentalization of PEI-modified polymeric nanospheres in PC12 cells. In all panels, solid points represent free nanospheres and open points cell-bound nanospheres. (a) Decrease in r2 for cell-bound nanospheres compared with free nanospheres. (b) Decrease in r1 following internalization of nanospheres. (c) Effect of echo spacing (TE) on R2 relaxation rate. Top panel: Similar values of r2 for free nanospheres using short (triangles) and long (stars) TE. Bottom panel: Nanospheres compartmentalized within cells display a doubling in r2 between short (triangles) and long (stars) echo time measurements. (d) Reduced dependence of r1 on field for compartmentalized (open) compared with free (solid) particles.

in a larger population of cells using relaxometry. This analysis was made possible by the superparamagnetic iron oxide nanoparticles contained within the nanospheres. Superparamagnetic nanoparticles are effective contrast agents for magnetic resonance (MR) imaging, as they possess a large magnetic moment and are free to align with an applied magnetic field. The resultant microscopic field gradients dephase nearby protons, shortening both the longitudinal relaxation time T1 and the transverse relaxation time T2. T1 is also reduced *via* other relaxation mechanisms. The corresponding relaxation rates, R1 and R2, are influenced by the local concentration of nanoparticles, the applied field strength, and the environment in which the nanoparticles interact with surrounding protons.[41−44] In particular, the relaxation induced by iron oxide nanoparticles is known to depend on their compartmentalization in macrophages, lymphocytes, oligodendrocytes, human neural stem cells, and mesenchymal stem cells.[41−46]

We analyzed relaxation rates in PC12 cells after 72 h exposure, by which time PEI-modified nanospheres were bound within intracellular compartments. We compared relaxation rates of nanospheres that had been endocytosed by PC12 cells with those of free nanospheres, both of which were held in agarose gels. The transverse relaxivity of free nanospheres at 1.4 T was $r2_{free}$ = 322 ± 26 mM^{-1} s^{-1} with a 19-fold reduction in PC12 cells ($r2_{cell}$ = 16.7 ± 1.2 mM^{-1} s^{-1}; Figure 4a). There was a 2-fold decrease in the longitudinal relaxivity r1 ($r1_{free}$ = 4.70 ± 0.05 mM^{-1} s^{-1}, $r1_{cell}$ = 2.70 ± 0.26 mM^{-1} s^{-1}; Figure 4b). The decrease in r2 on compartmentalization of nanospheres is attributed to the behavior of the aggregates as a micrometric nanosphere. The larger effective diameter shifts the compartmentalized nanoparticles into the echo-limited proton relaxation regime.[47] In this echo-limited environment, the perturbations in the magnetic field experienced by the water protons become effectively static. Hence, the refocusing pulses become efficient, reducing r2 compared to the dispersed nanoparticles and introducing a significant dependency on the echo spacing (Figure 4c). Furthermore, the dramatic dependence of r1 on magnetic field strength (Figure 4d) is also consistent with clustering of the nanoparticles and similar to theoretical predictions and observations.[48] We attribute the reduction in r1 to the less rapid inner-sphere exchange of water molecules inside the cell as well as a reduced molecular exchange with bulk water through a "membrane-shielding" effect.[45]

Using fluorescence intensity as a measure of iron content, we would expect that the state of clustering within cells could be measured over time using relaxometry. This advantage of the multimodal nanospheres will be helpful in following endolysosomal sorting not only *in vitro* but also on a larger scale *in vivo* using live fluorescence imaging in conjunction with MRI. A standard curve of fluorescence *versus* iron content was

constructed with strong correlation (r = 0.9970), from which we were able to determine the iron content of a cellular sample to within 10% error (Figure S8).

CONCLUSION

The nanospheres used in the present study represent a novel combination of features including direct visualization by electron and fluorescence microscopy, as well as the ability to examine compartmentalization after endocytosis by relaxometry. The magnetic properties also enabled removal of excess PEI, enabling examination of PEI-mediated endocytosis without the confounder of toxicity of free PEI. Endocytosis involved a clear sequence of events: interaction of nanoparticles with the cell membrane induced membrane ruffling and tubular invagination, characteristic respectively of unregulated/unselective macropinocytosis and clathrin- and caveolin-independent endocytosis, followed by time-dependent intracellular clustering within lamellar envelopes. The nanosphere architecture thus offers a broad scope for delivery of a wide range of agents to intracellular compartments. The findings we have presented will assist in the design and synthesis of next-generation nanoparticles for site-specific drug delivery.

MATERIALS AND METHODS

Materials. All chemicals were purchased from Sigma-Aldrich unless otherwise stated: benzyl ether (99%), chlorpromazine hydrochloride (98%), 5-(*N*,*N*-dimethyl)amiloride hydrochloride, iron(III) acetylacetonate (97%), nystatin, oleic acid (BDH, 92%), oleyl amine (70%), Pluronic F-108, polyethylenimine (50% solution, M_n 1200, M_w 1300), progesterone (99%), rhodamine B (Kodak, 95%), and 1,2-tetradecanediol (90%) were used as received. All tissue culture reagents were purchased from Invitrogen unless otherwise stated: B27, bovine serum albumin (Aldrich), DMEM, fetal bovine serum, L-glutamine 200 mM, GlutaMAX 100×, horse serum, MEM, Neurobasal, nonessential amino acids (NEAA) 100×, penicillin/streptomycin, poly(L-lysine) (Aldrich), RPMI1640, sodium pyruvate 100×, and trypsin/EDTA. Samples were mounted for light microscopy using Fluoromount-G (Southern Biotech).

Preparation of Iron Oxide Nanoparticles. Fe_3O_4 was synthesized by the organic decomposition of $Fe(acac)_3$ in benzyl ether at 300 °C, in the presence of oleic acid, oleyl amine, and 1,2-tetradecanediol, as previously described.[49,50]

Synthesis of RhB-Modified PGMA. PGMA was synthesized by radical polymerization according to a published procedure.[22] In brief, glycidyl methacrylate was polymerized in methyl ethyl ketone (MEK) to give PGMA (M_w = 250 000 g mol^{-1}), using azobisisobutyronitrile as initiator. The polymer was purified by multiple precipitations from MEK solution using diethyl ether. To attach the dye to the polymer, a solution of rhodamine B (RhB, 20 mg) and PGMA (100 mg) in MEK (20 mL) was heated to reflux under N_2 for 18 h. The solution was reduced *in vacuo* before the modified polymer was precipitated with diethyl ether (20 mL). The polymer was redissolved in MEK and precipitated with ether twice to remove ungrafted RhB.

Polymer Nanosphere Preparation. Nanoparticles were prepared using a nonspontaneous emulsification route. The organic phase was prepared by dispersing iron oxide nanoparticles (20 mg) and dissolving PGMA–RhB (75 mg) in a 1:3 mixture of $CHCl_3$ and MEK (6 mL). The organic phase was added dropwise, with rapid stirring, to an aqueous solution of Pluronic F-108 (1.25% w/v, 30 mL), and the emulsion was homogenized with a probe-type ultrasonicator at low power for 1 min. The organic solvents were allowed to evaporate overnight under a slow flow of N_2. Centrifugation at 3000*g* for 45 min removed large aggregates of iron oxide and excess polymer. The supernatant was removed to a 50 mL flask containing PEI (50 wt % solution, 100 mg) and heated to 80 °C for 18 h. The magnetic polymeric nanospheres were collected on a magnetic separation column (LS, Miltenyi Biotec), washed with water (2 × 1.5 mL), and then flushed with water until the filtrate ran clear. The resulting concentrated particle suspension was aliquoted (*ca.* 10 × 500 μL) and stored at 4 °C for quantification by lyophilization, analysis, and subsequent use. Nanospheres were sterilized by UV irradiation.

Cell Culture. Rat pheochromocytoma cells (PC12) were obtained from the Mississippi Medical Center (Jackson, MS), cultured in poly-(L-lysine)-coated polystyrene flasks in a humidified atmosphere containing 5% CO_2 at 37 °C, and maintained in RPMI1640 medium containing horse serum (10% v/v), fetal bovine serum (5% v/v), penicillin/streptomycin (100 U mL^{-1}, 100 μg mL^{-1}), L-glutamine (2 mM), nonessential amino acids (100 μM), and sodium pyruvate (1 mM). For experiments, cells were seeded in 24- or 96-well plates or on glass coverslips coated with poly-(L-lysine) at a cell density of (0.5–2) × 10^5 mL^{-1} and incubated for 24 h prior to experiments. Cells were not differentiated. Retinal Müller cells (rMC-1) were cultured in uncoated polystyrene dishes in DMEM high-glucose medium containing fetal bovine serum (10%), penicillin/streptomycin (50 U mL^{-1}, 50 μg mL^{-1}), and L-glutamine (2 mM). Cells were seeded at 1 × 10^5 mL^{-1} and incubated for 24 h prior to experiments. Hippocampal and cortical neuronal cultures were prepared as follows and maintained for 7–14 days prior to experiments. All experiments were carried out in accordance with approved protocols from the Institutional Animal Care and Use Committee of the University of California, San Diego; procedures also conformed to "Principles of Laboratory Animal Care" (NIH publication No. 86-23, revised 1985) and were approved by The University of Western Australia's Animal Ethics Committee. Rat pups (Sprague–Dawley, P1; or PVG, P1–P3) were placed in a CO_2 atmosphere and rapidly decapitated or anesthetized with xylazine/ketamine (Ilium xylazil and Ketamil, Troy Laboratories, 10 and 50 mg kg^{-1}, respectively, ip) and euthanized with Euthal (pentobarbitone sodium 850 mg kg^{-1}, phenytoin sodium 125 mg kg^{-1}; ip). Brains were removed to a dish containing dissociation media [DM: in H_2O; $MgCl_2$, 5.8 mM; $CaCl_2$, 2.5 mM; HEPES, 1.6 mM; phenol red, 8 mg L^{-1}; Na_2SO_4, 90 mM; K_2SO_4, 18.75 mM] on ice, from which hippocampal and cortical tissue was isolated and removed to DM on ice. DM was removed, and prewarmed enzyme solution [ES: DM, 10 mL; papain, 200 U; L-cysteine, 1.6 mg] was added to the tissue, which was incubated at 37 °C for 25 min with gentle shaking every 5 min. The supernatant was replaced with heavy inhibitor [HI: DM, 12 mL; trypsin inhibitor, 120 mg; bovine serum albumin, 120 mg] for 2 min, then light inhibitor [LI: DM, 9 mL; HI, 1 mL] for 2 min, and then with plating media [PM: in Minimum Essential Medium; fetal bovine serum, 10% v/v; glucose, 20 mM; pen/strep, 20 U mL^{-1}, 20 μg mL^{-1}; GlutaMAX, 2 mM; sodium pyruvate, 1 mM] to a suitable dilution for cell counting. The tissue was triturated until a homogeneous cell suspension was obtained, and cells were further diluted and plated on glass coverslips coated with poly-(L-lysine) (10 μg mL^{-1}) overnight at 37 °C. Four hours later, PM was replaced with feeding media [FM: in Neurobasal; glucose, 12 mM; pen/strep, 20 U mL^{-1}, 20 μg mL^{-1}; GlutaMAX, 0.5 mM; B27, 2% v/v; 2-mercaptoethanol, 25 μM]. Half of the culture media was replaced twice weekly. Morphological assessment of primary cultures indicated that approximately 95% of cells were neuronal due to the initial serum-free conditions (n = 1000 cells assessed).

Cell Viability Measurements. Viability was measured using a Live/Dead cell kit (Invitrogen). Cells were incubated for 24 h before the cell media was replaced with nanoparticle suspensions of different concentrations in media. After a further 24 or 72 h, the nanoparticle suspension was removed, the cells were washed once with PBS, and 100 μL of Live/Dead reagents was

added (calcein AM, 1 μM; ethidium homodimer-1, 3 μM). After 30 min, images were recorded using an inverted fluorescence microscope at 20× magnification (Olympus IX-71, Olympus IX-81). Four images were recorded from each well at consistent locations for all wells and all experiments, and live and dead cells were counted. The trypan blue dye exclusion assay was used as an additional measure of cell viability, following similar treatment procedures. Cells were detached using trypsin−EDTA, resuspended in 100−200 μL of cell media, combined with trypan blue, and counted using a hemocytometer or an automated cell counter (Invitrogen Countess).

Endocytic Inhibition Study. PC12 cells were plated in 96-well plates as above. Solutions of chlorpromazine (10 μg mL^{-1}), nystatin, and progesterone (25 and 10 μg mL^{-1}, respectively), or 5-(*N*,*N*-dimethyl)amiloride (50 μM) were prepared in complete media; progesterone was diluted from a 2 mg mL^{-1} stock in EtOH. Cells were incubated for 1 h with inhibitors, and then the drugs were placed together with nanospheres (10 μg mL^{-1}). After 3 h, wells were washed with PBS and fluorescence was quantified (BMG FluoStar Optima).

Immunohistochemical Analysis. PC12 cells were grown as above, incubated with nanospheres (1−10 μg mL^{-1}) for 3, 6, 12, 24, or 72 h, and fixed in paraformaldehyde (4%). Fixed cells were incubated in PBS containing Triton X-100 (0.2%) and blocked (7.5%) for 10 min, then incubated in the same solution containing anti-LAMP1 (Abcam, 1:1000), anti-β-III-tubulin (Tuj-1, Chemicon, 1:500), and/or anti-GFAP (Dako, 1:1000) overnight. Antibodies and nuclei were visualized by incubation with Alexa 488 and/or Alexa 647 (Molecular Probes, 1:400) and Hoechst 33342 (Sigma, 1 μg mL^{-1}) for 1−2 h. Images were captured by confocal microscopy (Leica TCS SP2, Nikon A1Si).

Preparation of TEM Samples. PC12 cells were grown on 8 mm^2 or 1.2 mm diameter 50.8 μm Aclar film for chemical fixation or cryopreservation, respectively. The films were attached to the surface of 12-well culture plates by spot-welding and then UV-sterilized prior to the addition of cells. PC12 cells were plated as above and treated with nanospheres (10 μg mL^{-1}) for 3, 6, 12, 24, or 72 h prior to fixation or cryopreservation. Following chemical fixation (2.5% glutaraldehyde in PBS, pH 7.4), samples were rinsed with PBS and postfixed (1% OsO_4) prior to dehydration in a graded series of ethanol. Alternatively, cryopreservation was achieved by high-pressure freezing (Leica EM PACT2) after dipping sample discs in cryoprotectant (2 mg mL^{-1} low-gel agarose in cell media at 37 °C). Frozen samples were placed in freeze-substitution media (1% osmium tetroxide, 0.2% uranyl acetate, and 3% water in acetone) and gradually brought to room temperature in a freeze-substitution unit (Leica EM AFS2). All specimens were embedded in Procure-Araldite before sections (80−120 nm) were cut and collected on uncoated 200-mesh copper grids. Grids of conventionally processed specimens were stained with uranyl acetate and lead citrate prior to observation, while grids of high-pressure frozen specimens were unstained. Iron oxide and nanosphere samples were prepared for TEM by deposition on carbon-coated copper grids. All TEM images were obtained at 120 kV (JEOL JEM-2100).

Relaxometry. Relaxivity data were measured using four Minispec mq series instruments (Bruker) operating at 0.23, 0.46, 0.92, and 1.41 T. A Carl-Purcell-Meiboom-Gill (CPMG) spin echo sequence was used to measure T2. The echo spacing was 2 ms for the short TE measurements (1000 echoes) and 10 ms for the long TE measurements (200 echoes), with a repetition time of 10 s for both. An inversion recovery (IR) sequence was used to measure T1 using 10 inversion times (TI) logarithmically spaced between 50 and 5000 ms. One 75 cm^2 flask of PC12 cells was incubated with polymer nanospheres for 72 h at a concentration of 50 μg mL^{-1}. Cells were detached from the substrate, fixed in 4% paraformaldehyde, and counted before dilutions were prepared for relaxometry measurements. The samples were suspended in 0.5% agarose gel, and data were recorded at 37.5 °C. The iron content of the samples was determined by ICP-AES after acid digestion (5 mL).

Acknowledgment. We thank Prof. Giles Plant for helpful discussions, Prof. Jacqueline Phillips for the gift of PC12 cells, Greg Black for ICP sample preparation, and Leah Stone, Carole Bartlett, Michael Archer, Kim Nguyen-Ta, and Marie Davidson for technical assistance. This work was funded by the Australian Research Council (ARC), the National Health & Medical Research Council (NHMRC) of Australia, Perpetual (Philanthropy Australia) as administrators of the Sir Harry Secombe Trust, and the National Science Foundation (CBET-0756457). C.W.E. received an Australian Research Council Nanotechnology Network (ARCNN) Overseas Research Travel Fellowship. The authors acknowledge the Australian Microscopy & Microanalysis Research Facility at the Centre for Microscopy, Characterisation & Analysis, The University of Western Australia, funded by the University, State and Commonwealth Governments.

Supporting Information Available: Spectroscopic and magnetic data for nanospheres, cell viability and uptake data, chemical inhibition results, LAMP co-localization, and confocal time-lapse videos. This material is available free of charge *via* the Internet at http://pubs.acs.org.

REFERENCES AND NOTES

1. Rajendran, L.; Knolker, H. J.; Simons, K. Subcellular Targeting Strategies for Drug Design and Delivery. *Nat. Rev. Drug Discovery* **2010**, *9*, 29–42.
2. Sahay, G.; Alakhova, D. Y.; Kabanov, A. V. Endocytosis of Nanomedicines. *J. Controlled Release* **2010**, *145*, 182–195.
3. Duncan, R. The Dawning Era of Polymer Therapeutics. *Nat. Rev. Drug Discovery* **2003**, *2*, 347–360.
4. Nishikawa, T.; Iwakiri, N.; Kaneko, Y.; Taguchi, A.; Fukushima, K.; Mori, H.; Morone, N.; Kadokawa, J. Nitric Oxide Release in Human Aortic Endothelial Cells Mediated by Delivery of Amphiphilic Polysiloxane Nanoparticles to Caveolae. *Biomacromolecules* **2009**, *10*, 2074–2085.
5. Conner, S. D.; Schmid, S. L. Regulated Portals of Entry into the Cell. *Nature* **2003**, *422*, 37–44.
6. Doherty, G. J.; McMahon, H. T. Mechanisms of Endocytosis. *Annu. Rev. Biochem.* **2009**, *78*, 857–902.
7. Rejman, J.; Bragonzi, A.; Conese, M. Role of Clathrin- and Caveolae-Mediated Endocytosis in Gene Transfer Mediated by Lipo- and Polyplexes. *Mol. Ther.* **2005**, *12*, 468–474.
8. Yang, Z.; Sahay, G.; Sriadibhatla, S.; Kabanov, A. V. Amphiphilic Block Copolymers Enhance Cellular Uptake and Nuclear Entry of Polyplex-Delivered DNA. *Bioconjugate Chem.* **2008**, *19*, 1987–1994.
9. Lühmann, T.; Rimann, M.; Bitterman, A. G.; Hall, H. Cellular Uptake and Intracellular Pathways of PLL-*g*-PEG-DNA Nanoparticles. *Bioconjugate Chem.* **2008**, *19*, 1907–1916.
10. Alexis, F.; Lo, S. L.; Wang, S. Covalent Attachment of Low Molecular Weight Poly(ethylene imine) Improves Tat Peptide Mediated Gene Delivery. *Adv. Mater.* **2006**, *18*, 2174–2178.
11. Boussif, O.; Lezoualc'h, F.; Zanta, M. A.; Mergny, M. D.; Scherman, D.; Demeneix, B.; Behr, J. P. A Versatile Vector for Gene and Oligonucleotide Transfer into Cells in Culture and In Vivo: Polyethylenimine. *Proc. Natl. Acad. Sci. U. S. A.* **1995**, *92*, 7297–7301.
12. Akinc, A.; Thomas, M.; Klibanov, A. M.; Langer, R. Exploring Polyethylenimine-Mediated DNA Transfection and the Proton Sponge Hypothesis. *J. Gene Med.* **2005**, *7*, 657–663.
13. Sonawane, N. D.; Szoka, F. C.; Verkman, A. S. Chloride Accumulation and Swelling in Endosomes Enhances DNA Transfer by Polyamine-DNA Polyplexes. *J. Biol. Chem.* **2003**, *278*, 44826–44831.
14. Moghimi, S. M.; Symonds, P.; Murray, J. C.; Hunter, A. C.; Debska, G.; Szewczyk, A. A Two-Stage Poly(ethylenimine)-Mediated Cytotoxicity: Implications for Gene Transfer/Therapy. *Mol. Ther.* **2005**, *11*, 990–995.
15. Breunig, M.; Lungwitz, U.; Liebl, R.; Goepferich, A. Breaking up the Correlation between Efficacy and Toxicity for Nonviral Gene Delivery. *Proc. Natl. Acad. Sci. U. S. A.* **2007**, *104*, 14454–14459.
16. Bausinger, R.; von Gersdorff, K.; Braeckmans, K.; Ogris, M.; Wagner, E.; Brauchle, C.; Zumbusch, A. The Transport of

Nanosized Gene Carriers Unraveled by Live-Cell Imaging. *Angew. Chem., Int. Ed.* **2006**, *45*, 1568–1572.
17. Bright, N. A.; Gratian, M. J.; Luzio, J. P. Endocytic Delivery to Lysosomes Mediated by Concurrent Fusion and Kissing Events in Living Cells. *Curr. Biol.* **2005**, *15*, 360–365.
18. Harush-Frenkel, O.; Rozentur, E.; Benita, S.; Altschuler, Y. Surface Charge of Nanoparticles Determines Their Endocytic and Transcytotic Pathway in Polarized MDCK Cells. *Biomacromolecules* **2008**, *9*, 435–443.
19. Ivanov, A. I. Pharmacological Inhibition of Endocytic Pathways: Is It Specific Enough to Be Useful? In *Exocytosis and Endocytosis*, Ivanov, A. I., Ed.; Humana Press: Totowa, NJ, 2008; Vol. 440, pp 15−33.
20. Jin, H.; Heller, D. A.; Sharma, R.; Strano, M. S. Size-Dependent Cellular Uptake and Expulsion of Single-Walled Carbon Nanotubes: Single Particle Tracking and a Generic Uptake Model for Nanoparticles. *ACS Nano* **2009**, *3*, 149–158.
21. Yarar, D.; Waterman-Storer, C. M.; Schmid, S. L. A Dynamic Actin Cytoskeleton Functions at Multiple Stages of Clathrin-Mediated Endocytosis. *Mol. Biol. Cell* **2005**, *16*, 964–975.
22. Tsyalkovsky, V.; Klep, V.; Ramaratnam, K.; Lupitskyy, R.; Minko, S.; Luzinov, I. Fluorescent Reactive Core-Shell Composite Nanoparticles with a High Surface Concentration of Epoxy Functionalities. *Chem. Mater.* **2008**, *20*, 317–325.
23. Mislick, K. A.; Baldeschwieler, J. D. Evidence for the Role of Proteoglycans in Cation-Mediated Gene Transfer. *Proc. Natl. Acad. Sci. U. S. A.* **1996**, *93*, 12349–12354.
24. Li, H.; Shih, W. H.; Shih, W. Y.; Chen, L. Y.; Tseng, S. J.; Tang, S. C. Transfection of Aqueous CdS Quantum Dots Using Polyethylenimine. *Nanotechnology* **2008**, *19*, 475101.
25. Jiang, X. E.; Rocker, C.; Hafner, M.; Brandholt, S.; Dorlich, R. M.; Nienhaus, G. U. Endo- and Exocytosis of Zwitterionic Quantum Dot Nanoparticles by Live HeLa Cells. *ACS Nano* **2010**, *4*, 6787–6797.
26. Mayor, S.; Pagano, R. E. Pathways of Clathrin-Independent Endocytosis. *Nat. Rev. Mol. Cell Biol.* **2007**, *8*, 603–612.
27. Hufnagel, H.; Hakim, P.; Lima, A.; Hollfelder, F. Fluid Phase Endocytosis Contributes to Transfection of DNA by PEI-25. *Mol. Ther.* **2009**, *17*, 1411–1417.
28. von Gersdorff, K.; Sanders, N. N.; Vandenbroucke, R.; De Smedt, S. C.; Wagner, E.; Ogris, M. The Internalization Route Resulting in Successful Gene Expression Depends on Both Cell Line and Polyethylenimine Polyplex Type. *Mol. Ther.* **2006**, *14*, 745–753.
29. Rejman, J.; Conese, M.; Hoekstra, D. Gene Transfer by Means of Lipo- and Polyplexes: Role of Clathrin and Caveolae-Mediated Endocytosis. *J. Liposome Res.* **2006**, *16*, 237–247.
30. Poon, G. M. K.; Gariepy, J. Cell-Surface Proteoglycans as Molecular Portals for Cationic Peptide and Polymer Entry into Cells. *Biochem. Soc. Trans.* **2007**, *35*, 788–793.
31. Pichon, C.; Billiet, L.; Midoux, P. Chemical Vectors for Gene Delivery: Uptake and Intracellular Trafficking. *Curr. Opin. Biotechnol.* **2010**, *21*, 640–645.
32. Demeneix, B.; Behr, J.-P. Polyethylenimine (PEI). In *Advances in Genetics*; Huang, L.; Hung, M.-C.; Wagner, E., Eds.; Academic Press: San Diego, CA, 2005; Vol. 53, pp 215−230.
33. Mailänder, V.; Landfester, K. Interaction of Nanoparticles with Cells. *Biomacromolecules* **2009**, *10*, 2379–2400.
34. Marin, M. P.; Esteban-Pretel, G.; Ponsoda, X.; Romero, A. M.; Ballestin, R.; Lopez, C.; Megias, L.; Timoneda, J.; Molowny, A.; Canales, J. J.; Renau-Piqueras, J. Endocytosis in Cultured Neurons Is Altered by Chronic Alcohol Exposure. *Toxicol. Sci.* **2010**, *115*, 202–213.
35. Georgieva, J. V.; Kalicharan, D.; Couraud, P.-O.; Romero, I. A.; Weksler, B.; Hoekstra, D.; Zuhorn, I. S. Surface Characteristics of Nanoparticles Determine Their Intracellular Fate in and Processing by Human Blood-Brain Barrier Endothelial Cells in Vitro. *Mol. Ther.* **2011**, *19*, 318–325.
36. Grosse, S.; Aron, Y.; Thevenot, G.; Francois, D.; Monsigny, M.; Fajac, I. Potocytosis and Cellular Exit of Complexes as Cellular Pathways for Gene Delivery by Polycations. *J. Gene Med.* **2005**, *7*, 1275–1286.
37. Damm, E. M.; Pelkmans, L.; Kartenbeck, J.; Mezzacasa, A.; Kurzckalia, T.; Helenius, A. Clathrin- and Caveolin-1-Independent Endocytosis: Entry of Simian Virus 40 into Cells Devoid of Caveolae. *J. Cell Biol.* **2005**, *168*, 477–488.
38. Luzio, J. P.; Pryor, P. R.; Bright, N. A. Lysosomes: Fusion and Function. *Nat. Rev. Mol. Cell Biol.* **2007**, *8*, 622–632.
39. Van Meel, E.; Klumperman, J. Imaging and Imagination: Understanding the Endo-Lysosomal System. *Histochem. Cell Biol.* **2008**, *129*, 253–266.
40. Kichler, A.; Leborgne, C.; Coeytaux, E.; Danos, O. Polyethylenimine-Mediated Gene Delivery: A Mechanistic Study. *J. Gene Med.* **2001**, *3*, 135–144.
41. Billotey, C.; Wilhelm, C.; Devaud, M.; Bacri, J. C.; Bittoun, J.; Gazeau, F. Cell Internalization of Anionic Maghemite Nanoparticles: Quantitative Effect on Magnetic Resonance Imaging. *Magn. Reson. Med.* **2003**, *49*, 646–654.
42. Rad, A. M.; Arbab, A. S.; Iskander, A. S. M.; Jiang, Q.; Soltanian-Zadeh, H. Quantification of Superparamagnetic Iron Oxide (SPIO)-Labeled Cells Using MRI. *J. Magn. Reson. Imaging* **2007**, *26*, 366–374.
43. Kuhlpeter, R.; Dahnke, H.; Matuszewski, L.; Persigehl, T.; von Wallbrunn, A.; Allkemper, T.; Heindel, W. L.; Schaeffter, T.; Bremer, C. R2 and R2* Mapping for Sensing Cell-Bound Superparamagnetic Nanoparticles: In Vitro and Murine In Vivo Testing. *Radiology* **2007**, *245*, 449–457.
44. Simon, G. H.; Bauer, J.; Saborovski, O.; Fu, Y.; Corot, C.; Wendland, M. F.; Daldrup-Link, H. E. T1 and T2 Relaxivity of Intracellular and Extracellular USPIO at 1.5T and 3T Clinical MR Scanning. *Eur. Radiol.* **2006**, *16*, 738–745.
45. Bulte, J. W. M.; Douglas, T.; Witwer, B.; Zhang, S. C.; Strable, E.; Lewis, B. K.; Zywicke, H.; Miller, B.; van Gelderen, P.; Moskowitz, B. M.; Duncan, I. D.; Frank, J. A. Magnetodendrimers Allow Endosomal Magnetic Labeling and In Vivo Tracking of Stem Cells. *Nat. Biotechnol.* **2001**, *19*, 1141–1147.
46. Bulte, J. W. M.; Zhang, S. C.; van Gelderen, P.; Herynek, V.; Jordan, E. K.; Duncan, I. D.; Frank, J. A. Neurotransplantation of Magnetically Labeled Oligodendrocyte Progenitors: Magnetic Resonance Tracking of Cell Migration and Myelination. *Proc. Natl. Acad. Sci. U. S. A.* **1999**, *96*, 15256–15261.
47. Carroll, M. R. J.; Woodward, R. C.; House, M. J.; Teoh, W. Y.; Amal, R.; Hanley, T. L.; St Pierre, T. G. Experimental Validation of Proton Transverse Relaxivity Models for Superparamagnetic Nanoparticle MRI Contrast Agents. *Nanotechnology* **2010**, *21*, 035103.
48. Roch, A.; Gossuin, Y.; Muller, R. N.; Gillis, P. Superparamagnetic Colloid Suspensions: Water Magnetic Relaxation and Clustering. *J. Magn. Magn. Mater.* **2005**, *293*, 532–539.
49. Lattuada, M.; Hatton, T. A. Functionalization of Monodisperse Magnetic Nanoparticles. *Langmuir* **2007**, *23*, 2158–2168.
50. Sun, S. H.; Zeng, H.; Robinson, D. B.; Raoux, S.; Rice, P. M.; Wang, S. X.; Li, G. X. Monodisperse MFe_2O_4 (M = Fe, Co, Mn) Nanoparticles. *J. Am. Chem. Soc.* **2004**, *126*, 273–279.